Theoretical Model to Calculate Steady-State and Transient Ampacity and Temperature in Buried Cables

Carlos Garrido, Antonio F. Otero, and José Cidrás

***Abstract*—The temperature distribution and ampacity in a multilayered soil surrounding a system of three cables are calculated in the steady state and in emergency situations. In this paper, we present the mathematical model, which solves the heat diffusion equation in cylindrical coordinates inside the cables and in Cartesian coordinates in the surrounding soil. The finite difference method is used to solve the equations. In order to reduce the number of points studied that are of no interest to the results, a variable step discretization is used. Here, we present the development of the model and the effect of some of the parameters which influence the convergence and accuracy of the method. The application of the model in different configurations and situations is given in the second part of this work, sent for publication at the same time. The model is applicable to the study of buried cables in both the steady state and transient states for short-circuit and overload situations.**

***Index Terms*—Ampacity, thermal analysis, transient temperature, FDM, temperature rise.**

I. Introduction

In densely populated areas, electricity is usually transported and distributed through buried cables, due to the advantages that these offer compared to overhead cables. The main disadvantage of buried installations is knowing, with sufficient accuracy, the maximum values for ampacity that can flow through them in steady and transient states without insulation deterioration. This lack of knowledge is due to the temperature generated by the electrical current passing through the installation not being known accurately enough. The use of various material in the composition of the cables and the backfill in contact with them under certain conditions of use, can give rise to temperature increases above levels that the cable insulation can withstand without deterioration. As a consequence, under normal use, these installations are used below their real load possibilities. However, given the high cost of such installations, it would be useful to make optimum use of them so that the maximum possible current can circulate without exceeding the temperature limit for insulation deterioration. For this, it is necessary to know the temperature distribution around buried cables, the influence on this of the different elements making up the system, and the situations that can arise during use as accurately as possible.

Manuscript received December 13, 2000.

The authors are with the Department of Electrical Engineering, University of Vigo, Vigo, Spain (e-mail: garridos@uvigo.es).

Digital Object Identifier 10.1109/TPWRD.2002.801429

Analytical methods in conjunction with empirical approximations were initially used for the buried cable heat calculations [1]–[4]. Later, some writers took on the problem using a representation of the cable system by the thermal equivalent of a lump or distributed parameter electrical network [5], FFT techniques [6], Newton-Raphson techniques [7], etc. However, these are not the most suitable methods for a thorough temperature study. The invariability of the parameters with temperature, the excessive simplification of the geometry of the problem, and the materials and the starting conditions are some of the main minus points. Therefore, in order to predict the temperature distribution in buried cables as reliably as possible, one must resort to numerical calculation. Numerical methods can conveniently deal with the varying properties of the materials involved, the complexity of the real system, and the variability of the parameters with temperature. Different models have been presented that use finite difference methods [8]–[13], finite elements [14]–[19], or contour elements [21]. These methods represent the buried cable system by means of a discrete set of points and solve the heat diffusion equation using one of the discrete techniques mentioned. However, the models referred to do not show broad development which allows rapid application and, in many cases, are only applicable to the steady state. Similarly, none of them contemplates the variability of the parameters with temperature. In view of this, we have deemed it convenient to develop a model that can be applied to steady and transient states and takes into account the dependence of the parameters on temperature, always bearing in mind that the model must be able to respond to the basic questions arising from designers and users of these installations, such as: what is the time duration permitted for a specified overload given certain operating conditions? What temperatures will there be after a specified overload given certain operating conditions? What is the maximum ampacity for the cables for a given period of time and specified system temperatures? etc. The aim of this work is to develop a more exact method for obtaining the steady and transient heat fields in buried cable insulations, one which allows graphs or charts to be drawn up for different configurations and situations for easy application by electrical engineers. The model presented here is based on the finite difference method (FDM). Due to the length of the insulations, the model is independent of this variable, which means that only a two-dimensional (2-D) study of the problem is needed. One of the inconveniences that may arise is the need to consider a large area of study around the cables so as to guarantee that the furthermost points in the soil see no temperature modification (constant tem-

perature isotherms at points far enough from the cables). This normally leads to a compromise between choosing a number of study points which is not so great and choosing an isotherm in a position which does not correspond to it. To avoid this problem, Hanna *et al.* [8] introduced a restriction based on the law of energy conservation, by which they establish that heat losses through the limit area must be equal to the heat dissipated from the cables. This restriction permits a reduction in the size of the area under study but introduces new disadvantages. In our case, we have considered that in order to better tackle the problem, it is necessary to consider the whole area that is affected by heat increases. This means that to reduce the number of points, we have introduced a variable step discretization; thus, we can focus our attention (a greater number of study points) on the interior of the cables and the areas near these, while the areas further away (a lower temperature variation) is represented by a smaller number of discrete points. At the same time, the model includes the variability with temperature of the parameter involved (resistivity of the conductor and thermal conductivity and specific heat of the different materials in the cables and the soil). It is possible to simulate the moisture migration using a variable soil thermal conductivity as a function of the temperature. Also included are the heat losses to the environment through convection and gains through radiation. The model also considers dielectric losses, which may be great for medium or high voltages. The model is applied to temperature calculations in buried insulations and makes it possible to simulate calculations for direct current and alternating current by using different current values, etc.

Here, we present the model's mathematical development and the results concerning the model itself. In an accompanying work, the results obtained using our model for different usage conditions and different system configurations are shown.

II. Description of the Model

One of the most used configurations for buried power cables consists of three individual cables placed at the same level and with a typical separation between them of one diameter (Fig. 1). These cables are usually buried directly in the earth or in a backfill material such as concrete or sand. Alternatively, they are placed in pipes. In order to obtain the heat distribution around the buried cables, it is necessary to solve the heat diffusion equation

$$\rho Cp\frac{\partial T}{\partial t} = \nabla[K\nabla T] + Q \tag{1}$$

where ρ, Cp and K are, respectively, the density, the specific heat, and the thermal conductivity of the material being studied. Q represents the energy generation per time unit and volume unit. Both Cp and K usually vary with temperature. Likewise, heat generation, Q, varies from point to point and is a function of the temperature. Given that the length of the installation is much greater than the lateral dimensions, the above equation is considered independent of the length coordinate, so the equation is solved in a plane that is perpendicular to the length. Bearing in mind the geometry that is shown in Fig. 1, and with the aim of obtaining greater accuracy in the results, we use (1) in cylindrical coordinates inside the cables (made up of conductor, insulator, jackets, shield, sheath, etc.) and in Cartesian coordinates

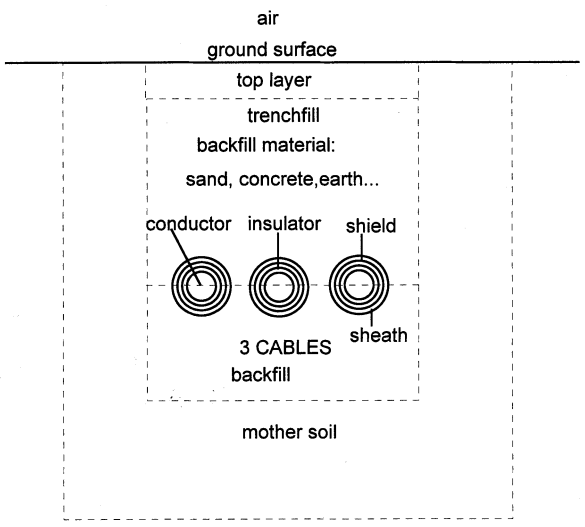

Fig. 1. Geometric model (cross–section) of a typical buried cable installation.

in the surrounding material. Putting the divergence and gradient operators through (1), and taking into account the variation with temperature of thermal conductivity, we obtain for cylindrical coordinates

$$\rho Cp\frac{\partial T}{\partial t} = \frac{K}{r}\frac{\partial T}{\partial r} + K\left[\frac{\partial^2 T}{\partial r^2} + \frac{\partial^2 T}{r^2\partial\theta^2}\right] + \frac{\partial K}{\partial T}\left[\left(\frac{\partial T}{\partial r}\right)^2 + \left(\frac{\partial T}{r\partial\theta}\right)^2\right] + Q \tag{2}$$

and for Cartesian coordinates

$$\rho Cp\frac{\partial T}{\partial t} = K\left[\frac{\partial^2 T}{\partial x^2} + \frac{\partial^2 T}{\partial y^2}\right] + \frac{\partial K}{\partial T}\left[\left(\frac{\partial T}{\partial x}\right)^2 + \left(\frac{\partial T}{\partial y}\right)^2\right] + Q. \tag{3}$$

Equations (2) and (3) are subject to the following boundary conditions:

a) In the soil which is far enough away from the cables, both to the sides and underneath, the temperature is not affected by the cables' presence, which means that in these areas, a temperature isotherm (T) is considered to be equal to the ambient soil temperature (T_T)

$$T = T_T = Cte. \tag{4}$$

b) At the separation surface between soil and air, convection losses are considered, which means that temperatures at this surface are obtained by taking into account Newton's law

$$\nabla(KT) = h(T - T_A) \tag{5}$$

where K is the thermal conductivity of soil (or material in the surface), h is the convective heat transfer coefficient (W/m$^2\cdot$°C), T is the temperature at the surface, and T_A is the air temperature.

c) In the separation between the different materials of the cable, between the surface of the cables and the surrounding medium, and between the different materials surrounding the cables, calorific flow continuity is fulfilled at the separation surface:

$$K_1 \frac{\partial T}{\partial l} = K_2 \frac{\partial T}{\partial l} \tag{6}$$

where l is the normal to the separation surface, and K_1 and K_2 represent the thermal conductivities of medium 1 and medium 2, respectively. Likewise, the temperature in both materials at the border points must be the same.

In (2) and (3), Q represents the heat generated per time unit and volume unit. The production of heat in the cable is due to current circulating through the conductors, jackets, and shields. At the same time, it is also necessary to consider the heat produced by dielectric losses, which can be great in medium and high voltages. To determine these losses, the formulae given in [22] are used. At the surface of the soil, the generation or loss of heat through radiation and the solar radiation must be considered. Heat generation from current circulation is given by

$$Q = \frac{R_p I_p^2}{\Delta V} \tag{7}$$

where R_p is the resistance of the section being considered, I_p is the current passing through that section, and ΔV is the volume. Taking into account the relationship between R_p and the resistivity of the conductor and the system of coordinates being used, we obtain, for each conductor

$$Q = \lambda \frac{I^2}{S^2} \tag{8}$$

where λ is the conductor's electrical resistivity, I is the total current passing through it, and S is its section. Electrical resistivity is assumed to be variable with temperature, and the effects on this of skin and proximity effects [22] have been taken into account. Both direct and alternating currents can be used in the model, and different current values for each conductor can also be used.

Given that (2) and (3) are nonlinear, their resolution cannot be undertaken using simple analytical techniques, which means we have approximated the partial derivatives using finite differences (FDM) [23]. The method consists of making a partition (Fig. 2) using a mesh of discrete points (i, j) where the temperature at each point is calculated to solve the equations that result from the approximations for (2) and (3) by finite differences, taking into account the applicable boundary conditions for each case. In this method, the speed of solution increases as the number of points studied decreases. However, the more points considered, the greater the accuracy. It is clear that at the points sited within the cables and their immediate surroundings, there is a greater heat gradient, which means that in these areas it is necessary to calculate the temperature at the highest possible number of points so as to obtain the most reliable results. Inversely, the areas further away from the cables have a smaller thermal gradient, which means the accuracy of the method is not compromised if the number of points chosen there is smaller. On the other hand, taking into account that the current limit (ampacity) is a consequence of the maximum temperature that the

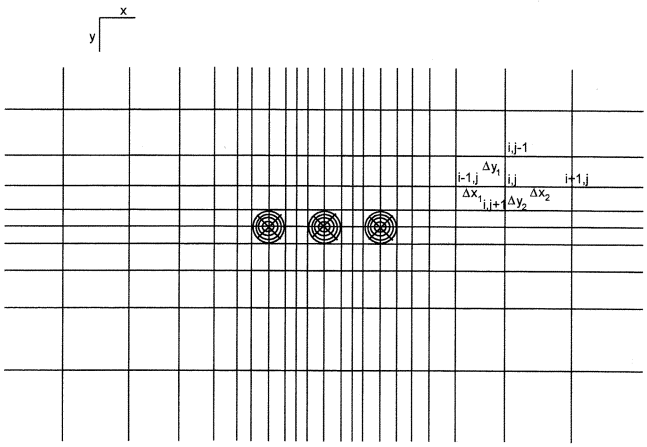

Fig. 2. Discretization employed.

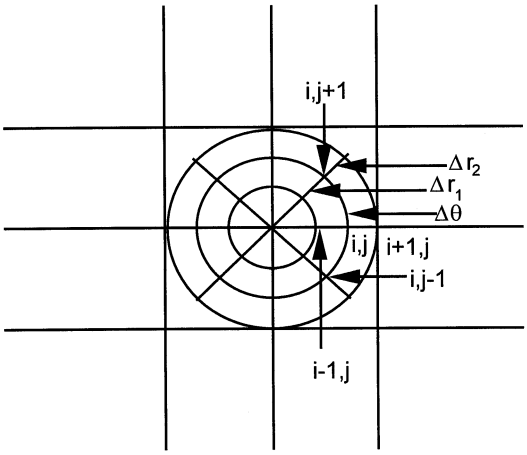

Fig. 3. Discretization inside the cables.

cable insulators can withstand without deteriorating, it is clear that a greater number of discrete points are needed from inside and nearby the cable for greater accuracy when calculating this limit. As a consequence of this, and with the aim of improving the speed without losing accuracy, we have approximated the partial derivatives through variable step finite differences [23] increasing the discretization step as we move away from the areas near the cables (see Fig. 2).

Applying variable step discretization to (2) and (3), we get cylindrical coordinates (see Fig. 3)

$$\begin{aligned}
&\frac{K}{2r}\left[\frac{T_{i,j}-T_{i-1,j}}{\Delta r_1}+\frac{T_{i+1,j}-T_{i,j}}{\Delta r_2}\right] \\
&\quad +2K\left[\frac{T_{i-1,j}}{\Delta r_1(\Delta r_1+\Delta r_2)}-\frac{T_{i,j}}{\Delta r_1 \Delta r_2}+\frac{T_{i+1,j}}{\Delta r_2(\Delta r_1+\Delta r_2)}\right] \\
&\quad +\frac{K}{r^2}\left[\frac{T_{i,j-1j}-2T_{i,j}+T_{i,j+1}}{\Delta\theta^2}\right] \\
&\quad +\frac{1}{2}\frac{\partial K}{\partial T}\left[\left(\frac{T^0_{i,j}-T^0_{i-1,j}}{\Delta r_1}\right)^2+\left(\frac{T^0_{i+1,j}-T^0_{i,j}}{\Delta r_2}\right)^2\right] \\
&\quad +\frac{1}{r^2}\frac{\partial K}{\partial T}\left[\frac{T^0_{i,j+1}-T^0_{i,j-1}}{2\Delta\theta}\right]^2+Q=\rho C_p\frac{T_{i,j}-T^0_{i,j}}{\Delta t}
\end{aligned} \tag{9}$$

where i and j represent, respectively, the discrete variables at coordinates r and θ.

Cartesian coordinates (see Fig. 2)

$$2K\left[\frac{T_{i-1,j}}{\Delta x_1(\Delta x_1+\Delta x_2)}-\frac{T_{i,j}}{\Delta x_1\Delta x_2}+\frac{T_{i+1,j}}{\Delta x_2(\Delta x_1+\Delta x_2)}+\frac{T_{i,j-1}}{\Delta y_1(\Delta y_1+\Delta y_2)}-\frac{T_{i,j}}{\Delta y_1\Delta y_2}+\frac{T_{i,j+1}}{\Delta y_2(\Delta y_1+\Delta y_2)}\right]+\frac{1}{2}\frac{\partial K}{\partial T}\left[\left(\frac{T^0_{i,j}-T^0_{i-1,j}}{\Delta x_1}\right)^2+\left(\frac{T^0_{i+1,j}-T^0_{i,j}}{\Delta x_2}\right)^2+\left(\frac{T^0_{i,j}-T^0_{i,j-1}}{\Delta y_1}\right)^2+\left(\frac{T^0_{i,j+1}-T^0_{i,j}}{\Delta y_2}\right)^2\right]+Q=\rho C_p\frac{T_{i,j}-T^0_{i,j}}{\Delta t} \tag{10}$$

where i and j represent, respectively, the discrete variables at coordinates x and y. T^o represents the temperature at the previous instant in time and Δt is the time increment being considered. Due to the nonlinearity of the equations, the nonlinear terms are evaluated with the temperature values obtained in the previous time iteration.

Grouping terms in (9) and (10), the equation system $A(i,j)T_{i,j}+A(i+1,j)T_{i+1,j}+A(i-1,j)T_{i-1,j}+A(i,j+1)T_{i,j+1}+A(i,j-1)T_{i,j-1}=F(i,j)$, is obtained, whose independent coefficients and term are given by the following. For polar coordinates

$$A(i,j)=\frac{\rho C_p}{\Delta t}+\frac{K}{2r}\left(\frac{1}{\Delta r_2}-\frac{1}{\Delta r_1}\right)+\frac{2K}{\Delta r_1\Delta r_2}+\frac{2K}{r^2\Delta\theta^2}$$

$$A(i+1,j)=-K\left(\frac{2}{\Delta r_2(\Delta r_1+\Delta r_2)}+\frac{1}{2r\Delta r_2}\right)$$

$$A(i-1,j)=-K\left(\frac{2}{\Delta r_1(\Delta r_1+\Delta r_2)}-\frac{1}{2r\Delta r_1}\right)$$

$$A(i,j+1)=-\frac{K}{r^2\Delta\theta^2},\quad A(i,j-1)=-\frac{K}{r^2\Delta\theta^2}$$

$$F(i,j)=Q+\frac{\rho C_p T^0_{i,j}}{\Delta t}+\frac{1}{2}\frac{\partial K}{\partial T}\left[\left(\frac{T^0_{i,j}-T^0_{i-1,j}}{\Delta r_1}\right)^2+\left(\frac{T^0_{i+1,j}-T^0_{i,j}}{\Delta r_2}\right)^2\right]+\frac{1}{r^2}\frac{\partial K}{\partial T}\times\left[\frac{T^0_{i,j+1}-T^0_{i,j-1}}{2\Delta\theta}\right]^2 \tag{11}$$

and for Cartesian coordinates

$$A(i,j)=\frac{\rho C_p}{\Delta t}+2K\left(\frac{1}{\Delta x_1\Delta x_2}+\frac{1}{\Delta y_1\Delta y_2}\right),$$

$$A(i+1,j)=-\frac{2K}{\Delta x_2(\Delta x_1+\Delta x_2)}$$

$$A(i-1,j)=-\frac{2K}{\Delta x_1(\Delta x_1+\Delta x_2)}$$

$$A(i,j+1)=-\frac{2K}{\Delta y_2(\Delta y_1+\Delta y_2)},$$

$$A(i,j-1)=-\frac{2K}{\Delta y_1(\Delta y_1+\Delta y_2)}$$

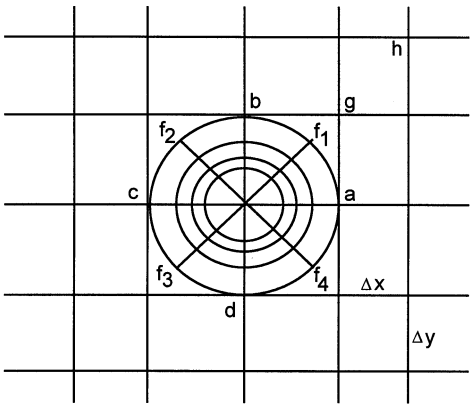

Fig. 4. Connection points between both systems.

$$F(i,j)=Q+\frac{\rho C_p T^0_{i,j}}{\Delta t}+\frac{1}{2}\frac{\partial K}{\partial T}\left[\left(\frac{T^0_{i,j}-T^0_{i-1,j}}{\Delta x_1}\right)^2+\left(\frac{T^0_{i+1,j}-T^0_{i,j}}{\Delta x_2}\right)^2+\left(\frac{T^0_{i,j}-T^0_{i,j-1}}{\Delta y_1}\right)^2+\left(\frac{T^0_{i,j+1}-T^0_{i,j}}{\Delta y_2}\right)^2\right]. \tag{12}$$

Should only the equation system for the steady state be needed, the terms containing Δt in the $A(i,j)$ and $F(i,j)$ coefficients can be eliminated from the previous equations.

In the previous equation system, the coefficients are a function of temperature, which depends on position and time. So in order to solve the equation system, we have used the over-relaxed iterative method (modified Gauss-Seidel) solved in an iterative way for each discrete time step Δt, thus obtaining the heat distribution over time. The connection between the equation system in cylindrical coordinates and the equation system in Cartesian coordinates is obtained through the four discrete points in common between the outer surface of the cable and the surrounding soil (discrete points a, b, c, and d in Fig. 4). However, for the temperature calculation in the surface separation between cable and soil at the points that are not in common between both coordinate systems (points f_1, f_2, f_3, f_4 in Fig. 4), a temperature is used that is obtained by interpolation between the nearest points in the soil in the radial direction (points g and h in the soil for point f_1). The interpolation chosen is due to its being more versatile when varying the values of Δx and/or Δy and this variation does not affect the results obtained with the model.

The discrete points where the boundary conditions given in (5) and (6) are fulfilled modify the equation system coefficients in accordance with what follows.

a) border points between different media

a.1) Separation surfaces between the different layers that make up the cable (conductor, insulation, shield, armor, jacket, sheath, etc.) and the soil or surrounding material. Bearing in mind that the following is fulfilled at the boundary points: $K_1(\partial T/\partial r)=K_2(\partial T/\partial r)$, with doing a Taylor development around point i sited on the boundary between both media: $T_{i+1,j}=$

$T_{i,j}+\Delta r(\partial T/\partial r)+(\Delta r^2/2)(\partial^2 T/\partial r^2), T_{i-1,j}=T_{i,j}-\Delta r(\partial T/\partial r)+(\Delta r^2/2)(\partial^2 T/\partial r^2)$ and clearing the second derivatives and substituting in the polar equation for both media (1 and 2) the following is obtained for the coefficients:

$$A(i,j)=\frac{\rho_1 C_{p1}}{c_1\Delta t}-\frac{\rho_2 C_{p2}}{c_2\Delta t}+\frac{2K_1}{c_1\Delta r_1^2}-\frac{2K_2}{c_2\Delta r_2^2}+\frac{2K_1}{c_1 r^2\Delta\theta^2}-\frac{2K_2}{c_2 r^2\Delta\theta^2},\quad A(i+1,j)=\frac{2K_2}{c_2\Delta r_2^2}$$

$$A(i-1,j)=\frac{2K_1}{c_1\Delta r_1^2},\quad A(i,j+1)=-\frac{K_1}{c_1 r^2\Delta\theta^2}+\frac{K_2}{c_2 r^2\Delta\theta^2}$$

$$A(i,j-1)=-\frac{K_1}{c_1 r^2\Delta\theta^2}+\frac{K_2}{c_2 r^2\Delta\theta^2}$$

$$F(i,j)=\frac{Q_1}{c_1}-\frac{Q_2}{c_2}+T^0_{i,j}\left(\frac{\rho_1 C_{p1}}{c_1\Delta t}-\frac{\rho_2 C_{p2}}{c_2\Delta t}\right)+\frac{1}{c_1}\frac{\partial K_1}{\partial T}\left(\frac{T^0_{i,j}-T^0_{i-1,j}}{\Delta r_1}\right)^2-\frac{1}{c_2}\frac{\partial K_2}{\partial T}\times\left(\frac{T^0_{i+1,j}-T^0_{i,j}}{\Delta r_2}\right)^2+\frac{1}{c_1 r^2}\frac{\partial K_1}{\partial T}\times\left[\frac{T^0_{i,j+1}-T^0_{i,j-1}}{2\Delta\theta}\right]^2-\frac{1}{c_2 r^2}\frac{\partial K_2}{\partial T}\left[\frac{T^0_{i,j+1}-T^0_{i,j-1}}{2\Delta\theta}\right]^2$$

where

$$c_1=\frac{1}{r}+\frac{2}{\Delta r_1}\quad\text{and}\quad c_2=\frac{1}{r}-\frac{2}{\Delta r_2}. \tag{13}$$

a.2) Separation surfaces between the different materials surrounding the cables (backfill material, top layer, and soil). As in the previous case, the boundary points fulfill $K_1(\partial T/\partial x)=K_2(\partial T/\partial x)$ or $K_1(\partial T/\partial y)=K_2(\partial T/\partial y)$ where x or y, respectively, are the normal to the separation surface, with a Taylor development around point i sited on the boundary between both media for the case where the surface separation is perpendicular to variable x:

$$T_{i+1,j}=T_{i,j}+\Delta x\frac{\partial T}{\partial x}+\frac{\Delta x^2}{2}\frac{\partial^2 T}{\partial x^2},$$
$$T_{i-1,j}=T_{i,j}-\Delta x\frac{\partial T}{\partial x}+\frac{\Delta x^2}{2}\frac{\partial^2 T}{\partial x^2}$$

and clearing the second derivatives and substituting in the Cartesian equation for both media (1 and 2) the following is obtained for the coefficients:

$$A(i,j)=\frac{\Delta x_1\rho_1 C_{p1}}{2\Delta t}+\frac{\Delta x_2\rho_2 C_{p2}}{2\Delta t}+\frac{\Delta x_1 K_1}{\Delta y_1\Delta y_2}+\frac{\Delta x_2 K_2}{\Delta y_1\Delta y_2}+\frac{K_1}{\Delta x_1}+\frac{K_2}{\Delta x_2}$$

$$A(i+1,j)=-\frac{K_2}{\Delta x_2}\quad A(i-1,j)=\frac{K_1}{\Delta x_1}$$

$$A(i,j+1)=-\frac{\Delta x_1 K_1+\Delta x_2 K_2}{\Delta y_1(\Delta y_1+\Delta y_2)}$$

$$A(i,j-1)=-\frac{\Delta x_1 K_1+\Delta x_2 K_2}{\Delta y_2(\Delta y_1+\Delta y_2)}$$

$$F(i,j)=T^0_{i,j}\left(\frac{\Delta x_1\rho_1 C_{p1}}{2\Delta t}+\frac{\Delta x_2\rho_2 C_{p2}}{2\Delta t}\right)+\frac{\Delta x_1}{2}\frac{\partial K_1}{\partial T}\left(\left(\frac{T^0_{i,j}-T^0_{i-1,j}}{\Delta x_1}\right)^2+\left(\frac{T^0_{i,j}-T^0_{i,j-1}}{\Delta y_1}\right)^2\right)+\frac{\Delta x_2}{2}\frac{\partial K_2}{\partial T}\times\left(\left(\frac{T^0_{i+1,j}-T^0_{i,j}}{\Delta x_2}\right)^2+\left(\frac{T^0_{i,j+1}-T^0_{i,j}}{\Delta y_2}\right)^2\right) \tag{14}$$

and similarly for the case where the separation surface is perpendicular to variable y.

a.3) Corner points between two materials in Cartesian coordinates

In the same way as the previous cases, the boundary points fulfill $K_1(\partial T/\partial x)=K_2(\partial T/\partial x)$ and $K_1(\partial T/\partial y)=K_2(\partial T/\partial y)$ where x and y, respectively, are the normal to the separation surface. With a Taylor development around point i sited on the boundary between both media for the case in which the separation surface is perpendicular to variable x: $T_{i+1,j}=T_{i,j}+\Delta x(\partial T/\partial x)+(\Delta x^2/2)(\partial^2 T/\partial x^2), T_{i-1,j}=T_{i,j}-\Delta x(\partial T/\partial x)+(\Delta x^2/2)(\partial^2 T/\partial x^2)$, clearing the second derivatives and substituting in the Cartesian equation for both media (1 and 2), the following is obtained for the coefficients (Fig. 5):

$$A(i,j)=\frac{\rho_1 C_{p1}(\Delta x_1\Delta y_1+\Delta x_2\Delta y_1+\Delta x_1\Delta y_2)}{2\Delta t}+\frac{\Delta x_2\Delta y_2\rho_2 C_{p2}}{2\Delta t}+K_1\left[\frac{\Delta y_1}{\Delta x_1}+\frac{\Delta x_1}{\Delta y_1}+\frac{\Delta y_1}{\Delta x_2}+\frac{\Delta x_2}{\Delta y_1}+\frac{\Delta y_2}{\Delta x_1}+\frac{\Delta x_1}{\Delta y_2}\right]+K_2\left[\frac{\Delta y_2}{\Delta x_2}+\frac{\Delta x_2}{\Delta y_2}\right]$$

$$A(i+1,j)-K_1\frac{\Delta y_1}{\Delta x_2}-K_2\frac{\Delta y_2}{\Delta x_2}$$

$$A(i-1,j)=-K_1\left[\frac{\Delta y_1}{\Delta x_1}+\frac{\Delta y_2}{\Delta x_1}\right]$$

$$A(i,j+1)=-K_1\frac{\Delta x_1}{\Delta y_2}-K_2\frac{\Delta x_2}{\Delta y_2}$$

$$A(i,j-1)=-K_1\left[\frac{\Delta x_1}{\Delta y_1}+\frac{\Delta x_2}{\Delta y_1}\right]$$

$$F(i,j)=T^0_{i,j}\left(\frac{\rho_1 C_{p1}(\Delta x_1\Delta y_1+\Delta x_2\Delta y_1+\Delta x_1\Delta y_2)}{2\Delta t}+\frac{\rho_2 C_{p2}\Delta x_2\Delta y_2}{2\Delta t}\right)+\frac{\Delta x_1\Delta y_1}{2}\frac{\partial K_1}{\partial T}\times\left(\left(\frac{T^0_{i,j}-T^0_{i-1,j}}{\Delta x_1}\right)^2+\left(\frac{T^0_{i,j}-T^0_{i,j-1}}{\Delta y_1}\right)^2\right)+\frac{\Delta x_2\Delta y_1}{2}\frac{\partial K_1}{\partial T}\left(\left(\frac{T^0_{i+1,j}-T^0_{i,j}}{\Delta x_2}\right)^2\right.$$

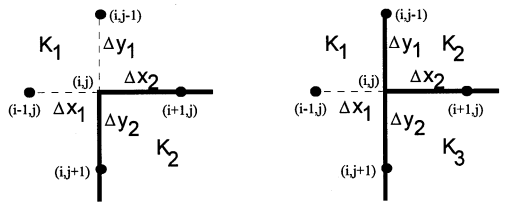

Fig. 5. Corner points between two materials and points between three materials.

$$+\left(\frac{T^0_{i,j}-T^0_{i,j-1}}{\Delta y_1}\right)^2\Bigg)+\frac{\Delta x_1\Delta y_2}{2}\frac{\partial K_1}{\partial T}\times\left(\left(\frac{T^0_{i,j}-T^0_{i-1,j}}{\Delta x_1}\right)^2+\left(\frac{T^0_{i,j+1}-T^0_{i,j}}{\Delta y_2}\right)^2\right)+\frac{\Delta x_2\Delta y_2}{2}\frac{\partial K_2}{\partial T}\left(\left(\frac{T^0_{i+1,j}-T^0_{i,j}}{\Delta x_2}\right)^2+\left(\frac{T^0_{i,j+1}-T^0_{i,j}}{\Delta y_2}\right)^2\right) \quad (15)$$

and similarly for the case where the separation surface is perpendicular to variable y.

a.4) Points between three materials in Cartesian coordinates. In the same way as the previous cases, the border points, calorific flow continuity is fulfilled at the separation surfaces. In a similar way, we obtain (Fig. 5)

$$\begin{aligned}
A(i,j)=&\frac{\rho_1C_{p1}(\Delta x_1\Delta y_1+\Delta x_1\Delta y_2)}{2\Delta t}+\frac{\Delta x_2\Delta y_1\rho_2C_{p2}}{2\Delta t}+\frac{\Delta x_2\Delta y_2\rho_3C_{p3}}{2\Delta t}+K_1\left[\frac{\Delta y_1}{\Delta x_1}+\frac{\Delta x_1}{\Delta y_1}+\frac{\Delta y_2}{\Delta x_1}+\frac{\Delta x_1}{\Delta y_2}\right]+K_2\left[\frac{\Delta y_1}{\Delta x_2}+\frac{\Delta x_2}{\Delta y_1}\right]+K_3\left[\frac{\Delta y_2}{\Delta x_2}+\frac{\Delta x_2}{\Delta y_2}\right]\\
A(i+1,j)=&-K_2\frac{\Delta y_1}{\Delta x_2}-K_3\frac{\Delta y_2}{\Delta x_2}\\
A(i-1,j)=&-K_1\left[\frac{\Delta y_1}{\Delta x_1}+\frac{\Delta y_2}{\Delta x_1}\right]\\
A(i,j+1)=&-K_2\frac{\Delta x_1}{\Delta y_2}-K_3\frac{\Delta x_2}{\Delta y_2}\\
A(i,j-1)=&-K_1\frac{\Delta x_1}{\Delta y_1}-K_2\frac{\Delta x_2}{\Delta y_1}\\
F(i,j)=&T^0_{i,j}\left(\frac{\rho_1C_{p1}(\Delta x_1\Delta y_1+\Delta x_1\Delta y_2)}{2\Delta t}+\frac{\rho_2C_{p2}\Delta x_2\Delta y_1}{2\Delta t}+\frac{\rho_3C_{p3}\Delta x_2\Delta y_2}{2\Delta t}\right)+\frac{\Delta x_1\Delta y_1}{2}\frac{\partial K_1}{\partial T}\left(\left(\frac{T^0_{i,j}-T^0_{i-1,j}}{\Delta x_1}\right)^2+\left(\frac{T^0_{i,j}-T^0_{i,j-1}}{\Delta y_1}\right)^2\right)+\frac{\Delta x_2\Delta y_1}{2}\frac{\partial K_2}{\partial T}\\
&\times\left(\left(\frac{T^0_{i+1,j}-T^0_{i,j}}{\Delta x_2}\right)^2+\left(\frac{T^0_{i,j}-T^0_{i,j-1}}{\Delta y_1}\right)^2\right)+\frac{\Delta x_1\Delta y_2}{2}\frac{\partial K_1}{\partial T}\left(\left(\frac{T^0_{i,j}-T^0_{i-1,j}}{\Delta x_1}\right)^2+\left(\frac{T^0_{i,j+1}-T^0_{i,j}}{\Delta y_2}\right)^2\right)+\frac{\Delta x_2\Delta y_2}{2}\frac{\partial K_3}{\partial T}\\
&\times\left(\left(\frac{T^0_{i+1,j}-T^0_{i,j}}{\Delta x_2}\right)^2+\left(\frac{T^0_{i,j+1}-T^0_{i,j}}{\Delta y_2}\right)^2\right).
\end{aligned} \quad (16)$$

b) Separation surface between the ground surface and the air. With a Taylor development on the border point (i,j), the separation surface being perpendicular to the coordinate y, if the second order derivative as a function of the first order derivative is obtained and taking into account the convection equation $\nabla(KT)=h(T-T_A)\Rightarrow K_T(\partial T/\partial y)=h(T-T_A)$, the following is obtained for the different coefficients:

$$\begin{aligned}
A(i,j)=&\frac{\rho_TC_{pT}}{\Delta t}+\frac{2K_T}{\Delta x_1\Delta x_2}+\frac{2K_T}{\Delta y_2^2}+\frac{2h}{\Delta y_2}\\
A(i+1,j)=&-\frac{2K_T}{\Delta x_2(\Delta x_1+\Delta x_2)}\\
A(i-1,j)=&-\frac{2K_T}{\Delta x_1(\Delta x_1+\Delta x_2)}\quad A(i,j+1)=-\frac{2K_T}{\Delta y_2^2}\\
A(i,j-1)=&-\frac{2h}{\Delta y_2},\quad F(i,j)=T^0_{i,j}\left(\frac{\rho_TC_{pT}}{\Delta t}\right)+\frac{\Delta y_2}{2}\frac{\partial K_T}{\partial T}\left(\left(\frac{T^0_{i,j+1}-T^0_{i,j}}{\Delta y_2}\right)^2+\left(\frac{T^0_{i+1,j}-T^0_{i,j}}{\Delta x_2}\right)^2\right)
\end{aligned} \quad (17)$$

where ρ_T, Cp_T, and K_T are, respectively, the density, the specific heat, and the thermal conductivity of soil.

III. Model Validation

In order to contrast the model, a known heat distribution, one corresponding to a determined heat generation Q, is introduced into it and the model's results are compared with those for the known distribution. In no case was the temperature calculation error greater than 0.2%. Likewise, for the transient model, if losses through the cable insulation are not taken into account, all of the heat generated goes into increasing the conductors' temperature, this increase can also be obtained through the adiabatic thermal equation [24]:

$$\Delta T=(T_i+\beta)\left[e^{\left(\frac{I^2t}{M^2S^2}\right)}-1\right] \quad (18)$$

where T_i is the initial temperature, I the current, M is a parameter that for copper is 226 A.s$^{1/2}$/mm^2, S is the conductor

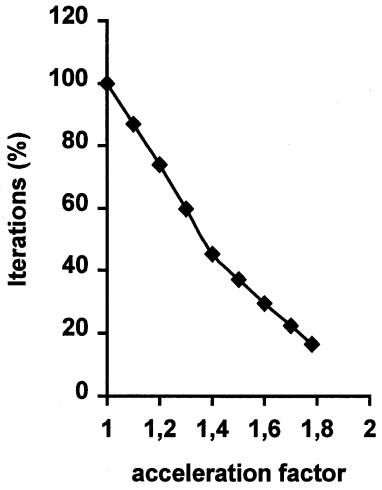

Fig. 6. Acceleration factor effect on the number of iterations.

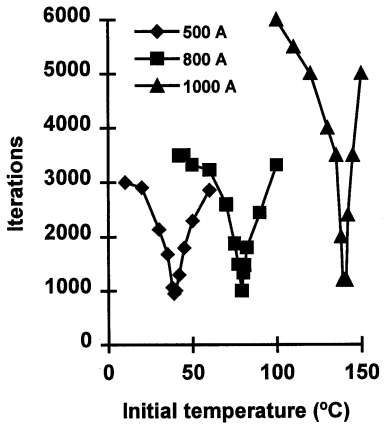

Fig. 7. Number of iterations as a function of initial temperature for the three currents.

section, and β is the inverse of the variation coefficient of the resistance.

In order to check its fitness, the temperatures were calculated assuming cable insulation with zero thermal conductivity so as to be able to compare it with (18). The study was carried out for cables with several cross–sections and with differing initial conditions for each case. The values obtained by our model coincide fully with the values obtained with the adiabatic equation.

IV. Results

Given that the Gauss-Seidel method is used to resolve the nonlinear equation system, it is interesting to estimate the acceleration factor ν in order to reduce as much as possible the number of iterations needed to reach convergence. Fig. 6 shows the number of iterations needed (as a percentage) to reach convergence according to the acceleration factor. The number of iterations needed with $\nu = 1$ represents 100%. It can be seen that the number of iterations needed is significantly reduced up to a value of 16% for $\nu = 1.78$. For values of ν over 1.78, the system becomes unstable. However, the total number of iterations is still quite high, although this number depends on the starting point (initial conditions) chosen for solving the system. In the steady state, unlike the model presented by Hanna *et al.* [8], the choice of initial temperature is not a critical parameter in the number of iterations to be carried out, as the model supports the introduction of a known heat distribution as an initial starting point. The more this distribution approaches that corresponding to the current being used, the lower the number of iterations needed to reach convergence is. However, we have also tested our model (in the steady state) assuming the same initial temperature at all of the discrete points. Clearly this situation is far removed from the final one, which means that the number of iterations needed to reach convergence is great. The number of iterations needed to reach convergence as a function of the initial temperature specified when beginning the calculation can be seen in Fig. 7. It can be observed that the initial temperature that needs to be specified in order to obtain the least number of iterations increases with the current passing through the cables. This is clear, because at greater currents, the temperature is higher also, which means that the starting temperature for reaching convergence in fewer iterations must also increase. For each current (that is, for each heat distribution), the number of iterations decreases with the increase in initial temperature until a minimum is reached, from which point the number of iterations needed to reach convergence increases again. Clearly, this result has to do with the final temperature attained, as a uniform initial temperature at all of the discrete points which represents the average value of the final temperature will give rise to the lowest number of iterations. However, in our model, in order to reduce the number of iterations as much as possible, the heat distribution corresponding to a current, near that for which temperature is being calculated, can be introduced as an initial temperature (initial condition). It should also be pointed out that the coefficients and terms that are independent of the equation system are modified in each iteration because they are themselves a function of the temperature. This can give rise to an increase in the number of iterations needed to reach convergence. In the case of steady–state calculations, the effect was studied of the independent coefficients and terms on the number of calculation iterations. In one case, they were calculated in each iteration, while in another they were calculated for the initial temperature values, the system was resolved, they were recalculated at the new temperatures, the system was again resolved, and they were recalculated again at the new temperatures, etc. until convergence was reached. After developing several examples for the different cases, we can conclude that the fastest resolution method is the one where the independent terms and coefficients are calculated in each iteration.

Once the convergence criterion has been chosen (temperature difference ΔT between two successive iterations), it is especially important to reduce the number of iterations and reach adequate accuracy. Thus, Fig. 8 shows the relationship between the convergence criterion ΔT and the absolute error in the final temperature for a system made up of three low–voltage conductors buried directly into the ground at a depth of 1000 mm and where the heat distribution corresponding to the steady state was studied for currents of 500, 800, and 1000 A. Thus, for $\Delta T = 10^{-6\circ}$ C, the least possible error was achieved. However, the method continues for an infinite number of iterations

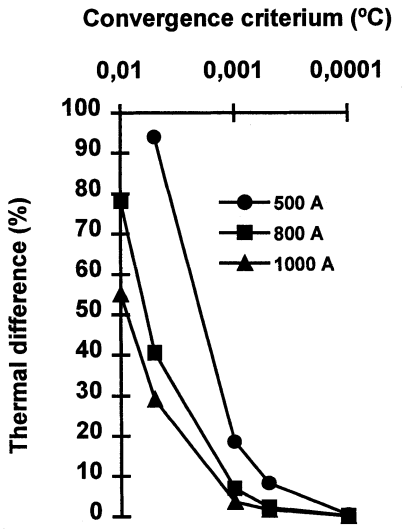

Fig. 8. Difference (in percent) between the final temperature and the real temperature according to the ΔT convergence criterion.

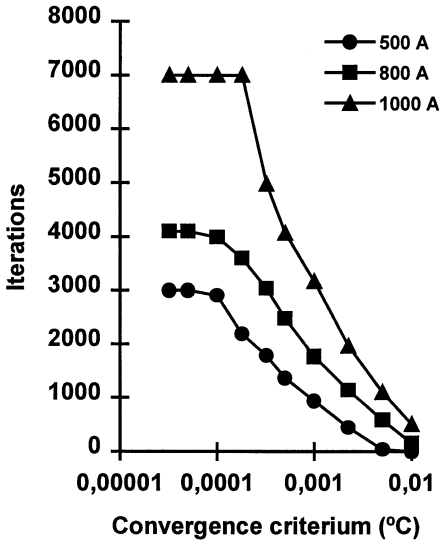

Fig. 9. Number of iterations needed to reach convergence according to the convergence criterion.

due to the calculation itself always being greater than the convergence criterion, with the temperature varying (after a sufficient number of iterations) between two values that only differ in the fifth decimal place. This value was taken as the true final temperature value. The error in the temperature estimation depends on the current passing through the cables and is greater when the current is lower. For values of $\Delta T \leq 10^{-5\circ}$ C, the system converges, and different final temperatures are obtained according to the ΔT value used. Thus, for $\Delta T = 10^{-5\circ}$ C, the same final temperature is obtained as for the ideal case, whereas, at the other extreme, for $\Delta T = 10^{-2\circ}$ C, temperature estimation errors of more than 50% are obtained. As can be deduced from the figure, in order to obtain calculation errors of less than 1%, it is necessary to use values of ΔT below $4 \times 10^{-4\circ}$ C. Fig. 9 shows the number of iterations needed to reach convergence for the three currents of 500, 800, and 1000 A from the

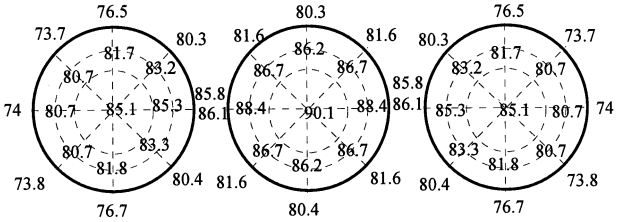

Fig. 10. Temperature distribution in the three cables.

previous case. From the figure, one can deduce that the greater the current (and, therefore, the temperature in the cables) and the smaller ΔT, the higher the number of iterations needed to reach convergence. On the other hand, according to the previous Fig. 8, there is a practically negligible reduction in the number of iterations for values of ΔT with which small errors in temperature calculation are obtained (curve section between 10^{-5} and $4 \times 10^{-4\circ}$ C).

The use of variable step discretization allows us to study the temperature inside cables and their immediate surroundings in full detail. For this, discretization intervals of less than 1 mm are used in the cables and the area next to them, whereas the discretization interval in distant areas is, in some cases, more than 1 m. It must be remembered that the greatest heat gradient takes place in the cables which means that calculating their temperature accurately needs a model that uses very small increments. In the areas further away, as the thermal gradient is very small, the use of large increments does not affect the thermal calculation. Partition of the soil is formed by a mesh of 33×21 discrete points while inside each cable the partition contains a total of 33 discrete points.

In Fig. 10, the temperature in three cables (500-mm^2 conductor section) buried directly in soil is shown when a current of 810 A circulates through them. The thermal conductivity of the soil is 0.915 W/m·° C, the convection coefficient is 7.38 W/m^2·° C and the ambient temperature is 20° C (in air and soil). It can be seen in the figure that the conductor of the central cable presents a temperature 5° C above that of the other two. In the insulator, the temperature is the same as that of the respective conductor, while the temperature in the sheath changes with position and distance. Thus, in the two outer cables, the temperature at the sheath surface varies from 85.8° C at the point nearest the central cable to 73.7° C at a point on the outer cable sheath nearly opposite the hottest point. The heat increase from the center of the cable to the surface of the sheath is approximately 10° C.

In Figs. 11 and 12, the temperature as a function of the distance to the center of the middle cable for different depths is shown. The parameters used are the same as those for the previous figure. Thus, Fig. 11 shows the temperature in the central cable and in the adjacent one in detail and how this reduces quickly once the soil is reached. As we approach the ground surface, the profiles are less marked, with the temperature at this surface (in the area located above the three cables) being 4.6°C above the environment temperature. Fig. 13 shows temperature as a function of depth (from the ground surface to the distance at which the soil isotherm is found below the cables). The parameters used are the same as those for the previous figures. The profiles shown correspond to different locations measured from

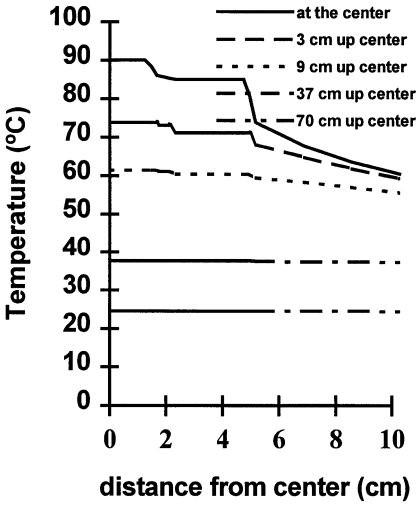

Fig. 11. Horizontal thermal profiles in the soil.

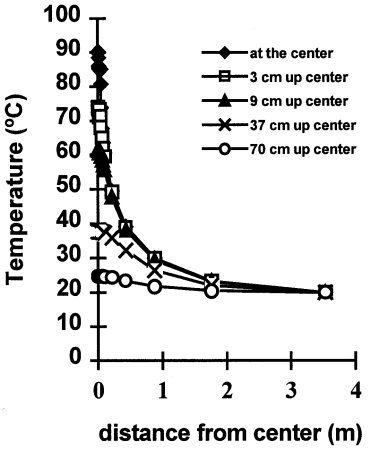

Fig. 12. Horizontal thermal profiles in the soil.

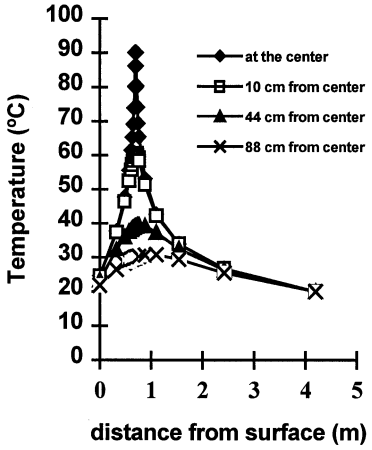

Fig. 13. Vertical thermal profile in the soil.

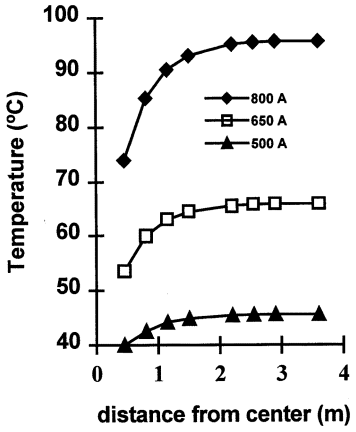

Fig. 14. Temperature in the central conductor as a function of the location distance of the ambient isotherm for different currents.

the center of the middle cable. Although the maximum temperature reached in the cables and in areas next to them is at the depth of the center of the cables (0.7 m), in areas of the soil that are further away, this maximum descends toward the interior of the soil in such a way that at a distance of 88 cm from the center the maximum is located at a depth of 1.1 m.

For model accuracy, it is important to establish the distance at which the isotherm is located from the cables, both sideways and downwards. In our case, the use of a discretization of variable step permitted us to study the position of this isotherm easily without having to increase the computation time. Fig. 14 shows the temperature that is obtained in the conductor of the central cable as a function of the distance (to the center of this cable) at which the isotherm is located, for three different values of current. In this figure, the cables are considered to be buried directly in the soil ($K = 0.833$ W/m·°C). The convection coefficient is $h = 7.38$ W/m^2°C and the ambient temperature is 25°C. The isotherm below the cables was located sufficiently far away so as not to affect the thermal distribution. As can be observed in the figure, the higher the temperature, the greater the influence of the isotherm's location. Nevertheless, so that the situation of the isotherm does not influence the result, it is necessary to locate it at more than 3.5 m from both sides of the central cable. The same conclusion is reached with respect to the location of the isotherm in the area below the cables. In order not to affect the temperature in the cables, it is necessary to locate the isotherm more than 3.5 m below the cables.

In Fig. 15, the effect that the thermal conductivity has on the location of the isotherm in the soil is shown. A current of 800 A has been assumed without change to the data from the previous figure. Clearly, the smaller the thermal conductivity of the soil is, the greater the temperature that is obtained in the cables. Therefore, the effect of the location of the isotherm is greater. In any case and even in the best conditions, it is necessary to locate the isotherm at distances greater than 3.5 m from the central cable in order not to affect the temperature calculation, and therefore, the estimation of ampacity for the system.

For the transient model, we have also checked how it is affected by the location of the isotherm in the soil. In this case, the influence isotherm location on admissible maximum short circuit duration has been studied (time needed to reach 250°C in the conductor). In Fig. 16, short circuit duration as a function of isotherm distance to the central cable is shown, for three short circuit currents. In this figure, the cables (500 mm^2 in conductor

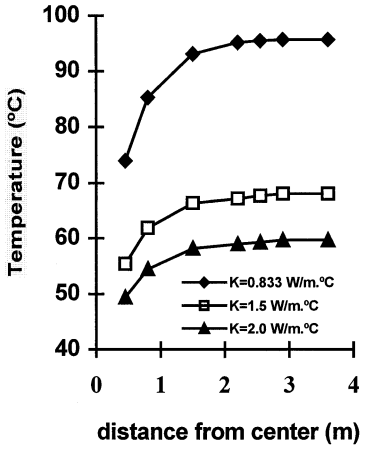

Fig. 15. Temperature in the central conductor as a function of the location distance of the ambient isotherm for different thermal conductivities in the soil.

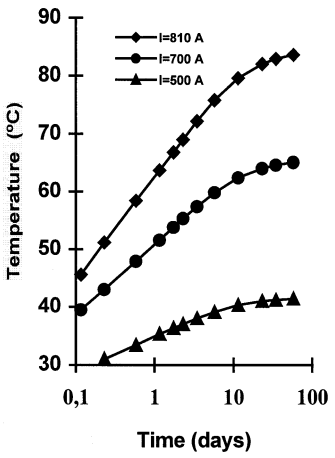

Fig. 17. Conductor temperatures as a function of time for different currents can be seen here.

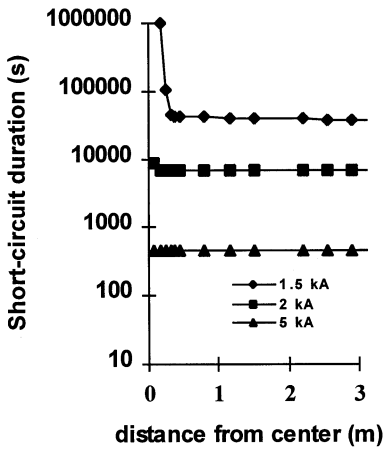

Fig. 16. Short circuit duration as a function of ambient isotherm location distance for different short circuit currents.

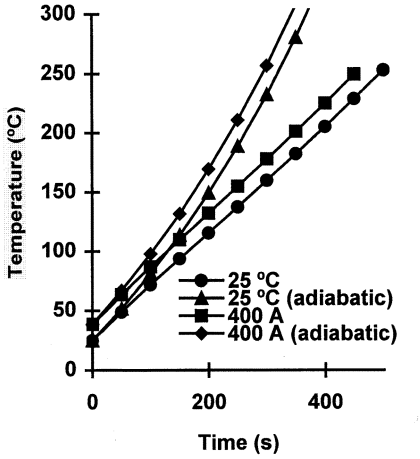

Fig. 18. Conductor temperatures as a function of time for different initial conditions compared with the adiabatic case.

section) are considered to be buried directly in soil ($K = 1$ W/m·°C). Convection coefficient is $h = 9.3$ W/m^2·°C and ambient temperature is 20°C. As can be observed in the figure, the location of the isotherm has less influence in this case than in the steady state. Only for a short circuit current of 1.5 kA, did isotherm location at a distance under 0.3 m noticeably modify short circuit duration. The 2–kA current is only affected in the case of an isotherm located at a distance of 0.2 m from the central cable. The 5–kA current is not affected by isotherm location, at least in the range of distances analyzed ($>$0.07 m). For currents below ampacity, isotherm location affects the time needed to reach final temperature as in the steady state.

In Fig. 17, temperature as a function of time is shown, for currents of 500, 700, and 810 A. Parameters are the same as for the previous figure. As an initial condition, soil and air ambient temperature at 20° C is assumed (cables without initial load). As can be observed, the temperature rose slowly with time until reaching the steady–state temperature. Taking into account time to reach steady state, variation in load and changes in ambient temperature, the temperature in buried cable system is actually a succession of a transient states.

It is usual, in the thermal study of conductors in short circuit situations, to calculate the heat increase with the adiabatic equation. With the sole aim of studying whether such an approach is conservative or not, we have carried out a series of calculations for the temperature in cables using our model and the adiabatic model. Fig. 18 shows some of the results gained for the three low voltage cables with 500-mm^2 conductor cross–section, insulation thickness (XLPE) of 2.2 mm, and sheath (PVC) thickness of 2 mm. The cables are in mutual contact and the burial depth (in simple soil) is 700 mm. The thermal conductivity of the soil is assumed at 0.833 W/m° C and the convection coefficient at 9.3 W/m^2° C. The figure shows the heat increase with our model and that calculated with the adiabatic model for two cases of different initial conditions. In the first case, it has been assumed that the cables and the soil together start at 25° C. In the second, the initial temperature corresponds to the heat distribution that exists for the steady state at a conductor current of 400 A (in this situation, the highest temperature is obtained from the central conductor cable where the value is 38.6° C). The short circuit current is 5000 A in both cases. The figure shows that the values obtained with the adiabatic model are much greater than

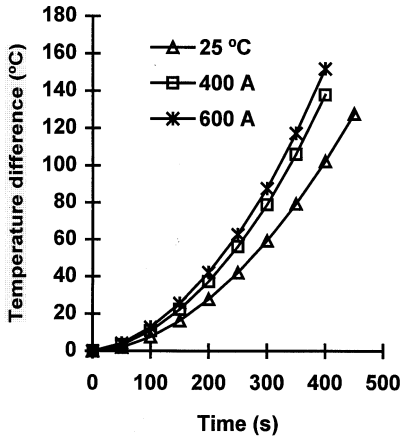

Fig. 19. Temperature difference between our model and the adiabatic method as a function of time.

those obtained with our model in both of the cases studied. The difference between the two models is increased as the short circuit duration time lengthens (and therefore, the temperature increases), with thermal differences over 100° C. The cases shown here clearly indicate that the adiabatic model is too conservative if the possibilities of the system are to be used to the maximum.

Fig. 19 shows the temperature differences obtained when comparing the results of our model with the adiabatic model for different three initial conditions at the start of the short circuit: a case corresponding to cables without load and ambient temperature of 25° C; and two other cases where steady–state temperature distributions for 400 and 600 A are assumed. The data corresponding to the cables and soil are the same as for Fig. 18. As expected, the difference is increased over time and with higher initial temperature conditions. This said, however, for the same temperature (which is reached in shorter times the higher the initial temperature) but with different initial conditions, the differences between the adiabatic model and our model are greater for those cases which begin with lower initial temperatures.

V. Conclusion

In this work, we have presented a model based on the finite difference technique in order to calculate the ampacity and the heat distribution in a buried, three-cable system. The model takes into account the various elements that make up the cables—conductor, insulation, shield, sheath, armor, etc.—along with the different possible materials that surround the cables. The fact that we have used a variable step discretization has allowed us to drastically reduce the number of points under study, and thus, simplify the problem that usually arises in this situation when a choice must be made between the best approximation and the least calculation effort. The model developed is applicable to steady and transient states, which means it can be used instead of the overly conservative adiabatic model to know the temperatures reached in the case of short circuits or overloads. The model enables the introduction of different initial conditions for each discrete point as well as the selection of adequate acceleration factors that can be used to reduce calculation time.

References

[1] D. M. Simmons, "Calculation of the electrical problems of underground cables," *Elect. J.*, vol. 29, no. 8, pp. 395–398, 1932.
[2] J. H. Neher and M. H. McGrath, "The calculation of the temperature rise and load capacity of cable systems," *Amer. Inst. Elect. Eng. Trans.*, pt. III, pp. 752–772, 1957.
[3] C. A. Bauer and R. J. Nease, "A study of the superposition of heat fields and the kennelly formula as applied to undergrounds cable systems," *Amer. Inst. Elect. Eng. Trans.*, pt. III, pp. 1330–1337, 1958.
[4] J. H. Neher and M. H. Magrath, "The calculation of the temperature rise and load capacity of cable systems," *Amer. Inst. Elect. Eng. Trans.*, pt. III, pp. 752–772, Oct. 1957.
[5] B. M. Weedy, "Air temperatures in a deep cable tunnel," *Elect. Power Syst. Res.*, vol. 15, pp. 229–232, 1988.
[6] G. C. Thomann *et al.*, "A fourier transform technique for calculating cable and pipe temperatures for periodic and transient conditions," *IEEE Trans. Power Delivery*, vol. 6, pp. 1345–1351, July 1991.
[7] T. A. Haskew, R. F. Carwile, and L. L. Gribsby, "An algorithm for steady-state thermal analysis of electrical cables with radiation by reduced Newton-Raphon techniques," *IEEE Trans. Power Delivery*, vol. 9, pp. 526–532, Jan. 1994.
[8] M. A. Hanna, A. Y. Chikhani, and M. A. A. Salama, "Thermal analysis of power cables in multi-layered soil—Part 1: Theoretical model," *IEEE Trans. Power Delivery*, vol. 8, pp. 761–776, July 1993.
[9] ——, "Thermal analysis of power cables in multi-layered soil—Part 2: Practical considerations," *IEEE Trans. Power Delivery*, vol. 8, pp. 772–778, July 1993.
[10] ——, "Thermal analysis of power cables in multi-layered soil—Part 3: Case of two cables in a trench," *IEEE Trans. Power Delivery*, vol. 9, pp. 572–578, Jan. 1994.
[11] W. Z. Black and S.-i. Park, "Emergency ampacities if direct buried three phase underground cables systems," *IEEE Trans. Power Apparat. Syst.*, vol. PAS-102, pp. 2124–2132, July 1983.
[12] B. M. Weedy, "An economic method for simulating the soil transient temperatures in a water cooled self-contained cable systems," *Elect. Power Syst. Res.*, vol. 14, pp. 207–217, 1988.
[13] A. Lombardi, F. Donazzi, C. Taralli, C. Tencer, and A. Lima, "Heat transfer in forced cooled cables," *IEEE Trans. Power Delivery*, vol. 5, pp. 8–13, Jan. 1990.
[14] J. K. Mitchell and O. N. Abdel-Hadi, "Temperature distribution around buried cables," *IEEE Trans. Power Apparat. Syst.*, vol. PAS-98, pp. 1158–1166, Apr. 1979.
[15] M. A. Kellow, "A numerical procedure for the calculation of the temperature rise and ampacity of underground cables," *IEEE Trans. Power Apparat. Syst.*, vol. PAS-100, pp. 3322–3330, July 1981.
[16] M. A. El-Kady, "Calculation of the sensitivity of power cable ampacity to variations of design and environmental parameters," *IEEE Trans. Power Apparat. Syst.*, vol. PAS-103, pp. 2043–2050, Aug. 1984.
[17] E. Tarasiewicz, E. Kuffel, and S. Grzybowski, "Calculation of temperature distribution within cable trench backfill and surrounding soil," *IEEE Trans. Power Apparat. Syst.*, vol. PAS-104, pp. 1973–1978, Aug. 1985.
[18] D. Mushamalirwa, N. Germay, and J. C. Steffens, "A 2-D finite element mesh generator for thermal analysis of underground power cables," *IEEE Trans. Power Delivery*, vol. 3, pp. 62–67, Jan. 1988.
[19] J. Lyall, "Two dimensional modeling of three core cable transient temperature rise," *IEEE Trans. Power Delivery*, vol. 5, pp. 21–25, Jan. 1990.
[20] G. Gela and J. J. Day, "Calculation of thermal field of underground cables using the boundary element method," *IEEE Trans. Power Delivery*, vol. 3, pp. 1341–1347, Oct. 1988.
[21] ——, "Using the boundary element method," in *Proc. IEEE/Power Eng. Soc. Winter Meeting*, New York, Jan. 31–Feb. 5 1988.
[22] Int. Electrotech. Comm., 2nd ed., Geneva, Switzerland, 1994. Pub. 287.
[23] J. P. Nougier, *Methodes de calcul numeérique*, 3rd ed, Paris, France: Masson, 1987.
[24] Int. Electrotechnical Commission, 2nd ed., Geneve, Switzerland, 1984. Pub. 724.

Carlos Garrido received the Ph.D. degree in physics from the University of Santiago de Compostela, Spain, in 1989.

Currently, he is Professor with the Department of Electrical Engineering at the University of Vigo, Spain. His main fields of interest are the measurement and characterization of magnetic fields and the thermal behavior of buried cables.

Antonio F. Otero received the Ph.D. degree in electrical engineering from the University of Vigo, Spain, in 1998.

Currently, he is a Professor with the Department of Electrical Engineering at the University of Vigo. His current research interest is magnetic fields and grounding systems.

José Cidrás received the Ph.D. degree in electrical engineering from the University of Santiago de Compostela, Spain, in 1987.

Currently, he is Professor and Head of the Department of Electrical Engineering at the University of Vigo, Spain, and leads investigation projects on wind energy, photovoltaics, planning of power systems, and magnetic fields.